

Upper-Level Frontogenesis Associated with the Birth of Mobile Troughs in Northwesterly Flow

DAVID M. SCHULTZ

NOAA/National Severe Storms Laboratory, Norman, Oklahoma

FREDERICK SANDERS

Marblehead, Massachusetts

(Manuscript received 28 October 2001, in final form 4 April 2002)

ABSTRACT

Previous studies have shown that 500-hPa mobile trough births (or genesis) occur preferentially in northwesterly flow during upper-level frontogenesis, and that cold advection assists in, and is a product of, mobile trough intensification. This study focuses on the synoptic environments and thermal-advection patterns of upper-level fronts associated with mobile trough births in northwesterly flow. A climatology of 186 such events, derived from an earlier study by Sanders, shows that most births tend to occur within uniform or diffluent flow and that most tend to be associated with relatively weaker 500-hPa thermal advection. Most mobile trough births in diffluence, however, tend to be associated with increasing 500-hPa cold advection, typically indicated by a cyclonic rotation of isentropes, whereas, most mobile trough births in confluence tend to be associated with weaker 500-hPa thermal advection.

Two cases of upper-level frontogenesis associated with mobile trough genesis—one in diffluence and one in confluence—are compared to determine the processes acting to produce the differing thermal-advection patterns at 500 hPa. A thermal-advection tendency equation is developed and shows that the magnitude of the temperature advection can be changed by accelerating the advecting wind speed or by changing the temperature gradient (i.e., vector frontogenesis). The latter can be accomplished either by changing the magnitude of the temperature gradient (the frontogenetical component F_n , also known as scalar frontogenesis) or by rotating the direction of the temperature gradient relative to the flow (the rotational component F_s). The dominant processes acting on F_n for the diffluence and confluence cases are tilting and deformation frontogenesis, respectively. The dominant process acting on F_s for the diffluence case is rotation of the isentropes due to the vorticity term, whereas rotation of the isentropes due to the vorticity and tilting terms are both important for the confluence case. The rotational component of frontogenesis is cyclonic downstream of the vorticity maximum for both cases, favoring increasing cold advection downstream of the vorticity maximum. For both cases, the rate of rotation of the isentropes at a point due to horizontal advection is large and that due to vertical advection is negligible. Since advection can only transport the existing isentrope angle and cannot change the isentrope angle, the rotational component of frontogenesis normalized by the temperature gradient is the only term that can increase the isentrope angle following the flow. This term dominates in the diffluence case but is small in the confluence case. This diagnosis suggests the following reasoning. In diffluent flow, the vorticity associated with the incipient trough is compacted into a more circular shape and intensifies. The potent vorticity maximum leads to robust isentrope rotation. In confluent flow, however, the vorticity is deformed into an elongated maximum, inhibiting both strong isentrope rotation and increasing cold advection. Thus, the rotational frontogenesis component explains the rotation of the isentropes that is responsible for the differing thermal-advection patterns.

Diagnosis of these cases supports the results from the climatology indicating a strong relationship between the synoptic environment and the upper-tropospheric thermal-advection pattern. Nevertheless, current conceptual models of upper-level frontogenesis do not fully explain the variety of these features in the real atmosphere. In particular, mobile trough genesis and its associated upper-level frontogenesis can occur in weak 500-hPa thermal-advection patterns, in contrast to the confluence and cold advection that have been previously identified as important to upper-level frontal intensification. This result provides further support for the possibility that generation and intensification of mobile troughs can occur by barotropic processes.

1. Introduction

Mobile troughs (shortwave troughs, cyclonic vorticity maxima, or, simply, vorticity maxima) are ubiquitous

within the upper-level westerlies (e.g., Hakim 2000). The question naturally arises as to their origin. As an initial approach, Sanders (1988) examined the position of the daily 0000 UTC 552-dam 500-hPa geopotential-height contour (isohypse) during nine cold seasons. The 500-hPa charts were from the National Meteorological Center (NMC), now known as the National Centers for Environmental Prediction (NCEP), Northern Hemi-

Corresponding author address: Dr. David M. Schultz, NOAA-National Severe Storms Laboratory, 1313 Halley Circle, Norman, OK 73069.
E-mail: schultz@nssl.noaa.gov

spheric analyses. Mobile trough locations along the 552-dam isohypse were identified and tracked; births and deaths, defined by Sanders as the first and last occurrence of curvature in the 552-dam isohypse, respectively, were also noted. Since troughs at 500 hPa typically are associated with tropopause-based disturbances, the disturbances likely already exist at lower pressures during mobile trough births. Therefore, mobile trough births at 500 hPa probably represent amplification of preexisting tropopause-based disturbances. Sanders (1988) found that trough births greatly exceeded trough deaths over and to the east of major mountain chains and when the 500-hPa geostrophic flow was northwesterly. These results were confirmed by Lefevre and Nielsen-Gammon (1995) and Dean and Bosart (1996) using automated vorticity-maxima tracking routines on the NMC Northern Hemispheric 500-hPa gridded analyses on compact disc (Mass et al. 1987).

Why northwesterly flow should be favored for mobile trough births (hereafter, also referred to as trough genesis) was explored by Lackmann et al. (1997, 1999). Based on a 12-event subset from a collection of 18 significant vorticity maxima during the Experiment on Rapidly Intensifying Cyclones over the Atlantic (ERICA) field phase, Lackmann et al. (1997) presented a characteristic life cycle associated with trough genesis, the so-called compactor life cycle. The term compactor describes the initially elongated disturbance that becomes more isotropic (compacts into a more circular shape, in other words, the length of the major axis of the vorticity maximum decreased relative to that of the minor axis). They showed that a developing mobile trough, initially elongated along northwesterly flow, was associated with frontogenesis along an upper-level baroclinic zone¹ because the vorticity of the trough was generated during tilting of the tropopause in association with upper-level frontogenesis, a concept originally discussed by Reed and Sanders (1953). The elongation of the front and vorticity maximum in the compactor life cycle is a result of the confluence orienting the axes of dilatation parallel to the flow, a point also noted by Wandishin et al. (2000, p. 3930). Lackmann et al. (1997) speculated that the presence of a downstream predecessor trough may have produced diffluence that aided the compacting process. Thus, an increase in circulation resulted from the reconfiguration of the potential vorticity anomaly, a process called superposition by Nielsen-Gammon (1995). Lackmann et al. (1999) summarized the evolution and energetics of such a mobile trough by noting that its intensification was due initially to barotropic processes that convert the kinetic energy of the jet stream to kinetic energy of the jet streak as-

sociated with the mobile trough. The associated transverse divergent circulations then favor upper-level frontogenesis and amplification of the vorticity maximum. The importance of downstream diffluence on trough amplification has been discussed further by Farrell (1989), Nielsen-Gammon (1995), and Nielsen-Gammon and Lefevre (1996). A complementary discussion of disturbance amplification by downstream development in northwesterly flow has been offered by Orlanski and Sheldon (1995).

Idealized two-dimensional model experiments (e.g., Shapiro 1981; Keyser and Pecnick 1985; Keyser et al. 1986; Reeder and Keyser 1988) have shown the importance of upper-tropospheric alongfront thermal advection toward the intensification of upper-level baroclinic zones. Specifically, the addition of upper-tropospheric cold advection to a background confluent flow field helps accelerate upper-level frontogenesis through a positive feedback that Rotunno et al. (1994) termed the Shapiro effect. The essence of the Shapiro effect is that, in the presence of cold advection and confluence, the cross-front ageostrophic circulation associated with the upper-level frontal zone becomes shifted toward warmer air, producing subsidence on the warm side of the frontal zone, favoring frontogenesis by tilting of the isentropes. In an idealized three-dimensional primitive-equation channel-model simulation of a growing normal mode, Rotunno et al. (1994) showed that the upper-level frontogenesis process initially proceeded from a small amount of horizontal-deformation frontogenesis, which led to frontogenetical tilting, in the absence of along-front cold advection. Later, they argued, descent of the isentropes produced alongfront cold advection, which, in combination with the confluence, resulted in the Shapiro effect and further frontal intensification. In contrast, for a case of upper-level frontogenesis and compaction over North America, Schultz and Doswell (1999) showed the transformation from a near-equivalent-barotropic stage (near-zero geostrophic thermal advection) to the cold-advection stage was attributed to the developing vorticity maximum associated with the upper-level frontogenesis, not descent of the isentropes. Keyser (1999, 254–257) and Schultz and Doswell (1999, p. 2558) have suggested that different processes may act when the front is forming [e.g., the linear stage of Rotunno et al. (1994)] compared to later when the front is more intense (e.g., the finite-amplitude stage), but this hypothesis remains to be tested.

Questions then arise as to 1) how representative the compactor life cycle is for trough genesis, 2) whether modes other than the compactor life cycle are possible for trough genesis in northwesterly flow, 3) how common the transformation from a near-equivalent-barotropic stage to cold-advection stage is for compactor events, and 4) the mechanism for the increasing cold advection along upper-level fronts.

To address these questions, in section 2, we perform a manual classification of trough genesis in 500-hPa

¹ Hereafter, we use the term upper-level front to apply to these upper-level baroclinic zones. In this context, the term front applies to a temperature gradient an order of magnitude larger than the background temperature gradient in the atmosphere (e.g., Bluestein 1993, p. 239), rather than an implied discontinuity of any order.

northwesterly flow over North America using data from Sanders's (1988) climatology of mobile troughs. This classification shows that troughs in 500-hPa diffluent flow are more likely to develop cold advection than troughs in confluent flow. We then select two representative events for further diagnosis: one in diffluence and one in confluence. Section 3 presents 500-hPa thermal-advection-tendency and vector-frontogenesis diagnostics to demonstrate why diffluence is favored over confluence for producing cold advection. The relationship of these results to those previously published on trough genesis is explored in section 4. Finally, section 5 presents a concluding summary.

2. Classification scheme

In order to compile a list of trough-genesis events in northwesterly flow, we examine the original 552-dam isohypse maps constructed by Sanders (1988). These maps were annotated with locations and dates of trough births according to the technique described in Sanders (1988). Each trough birth in northwesterly flow over North America between 30° and 60°N is identified by date and location. The flow was considered to be northwesterly (geostrophically) if the 552-dam isohypse on the upstream and downstream sides of the location of the trough birth had northwesterly orientations, or the orientation of the 552-dam isohypse on the upstream side of the trough was of equal or greater northwesterly orientation than that on the downstream side. This latter condition includes troughs born exiting northwesterly geostrophic flow into more zonal flow (e.g., Fig. 2). Sanders (1988, Table 1) constructed 552-dam isohypse maps for nine cold seasons. Since the publication of Sanders (1988), 1.5 more cold seasons have been analyzed: 12 September 1987–2 April 1988 and 1 October 1988–2 December 1988. During this 10.5-cold-season period, 186 trough births in northwesterly flow were identified from Sanders's maps.

Note that a trough birth according to the technique described by Sanders (1988) actually may not represent the true origin of the vorticity maximum. Sometimes troughs "migrate" to higher values of the geopotential height; for example, a preexisting trough in the 546-dam isohypse may later develop curvature in the 552-dam isohypse, a point discussed observationally by Sanders (1988, section 5e). This may be due to one of three possibilities. First, on the cyclonic-shear side of the jet, Rossby waves are refracted toward large potential vorticity gradients, as might be found along the axis of the jet (e.g., Karoly and Hoskins 1982). Second, equatorward-displaced vorticity maxima may intensify, resulting in an enlarged area of influence for the induced flow. Third, owing to the geometry of the 500-hPa surface relative to the tropopause, the tropopause slopes much more than adjacent isobaric surfaces, so the poleward side of the 500-hPa jet stream is closer to the tropopause than the equatorward side. Since 500-hPa

troughs usually accompany tropopause undulations, troughs at 500 hPa should be manifest earlier on the poleward side of the jet. No effort was made to eliminate these three lateral-migration effects from consideration. That automated absolute-vorticity tracking methods (Lefevre and Nielsen-Gammon 1995; Dean and Bosart 1996) have produced similar spatial climatologies to Sanders's (1988) manual method is a testament to the robustness of Sanders's (1988) results and the relatively small impact of this migration effect on the climatological statistics.

The historical NMC North American 500-hPa analyses on microfilm were then examined for each of the 186 events. Following two preliminary examinations of all 186 events, each event was characterized according to two criteria, based on these 500-hPa analyses only. First, a manual classification scheme was devised to categorize the synoptic environment in which the birth occurred: diffluent flow, confluent flow, uniform flow, trough fracture, closed low, or other. As noted by Sanders (1993), there may be some discrepancy between measuring deformation on the scale of the disturbance and that on the large scale. Although deformation was not explicitly computed for each event, the large-scale environment in which the mobile trough was embedded was manually determined to be *diffluent* or *confluent* if the 500-hPa isohypses spread or contracted, respectively, around and within about 1000 km downstream from the area where the trough was born according to Sanders's method (cf. Figs. 1a,b and 2a,b). (The ambiguity in the 1000-km value was imposed to allow some flexibility in accounting for the distribution in sizes of the mobile troughs.) The environment was classified as *uniform flow* if the isohypses were nearly parallel around and within about 1000 km downstream from the area of the trough birth (Fig. 3a). *Trough fracture* occurred when a single trough by Sanders's methodology became sufficiently elongated to form a closed low and a mobile counterpart in the poleward westerlies (Fig. 4). In this case, Sanders designated the mobile trough in the westerlies as the trough birth and the closed low retained the trough's designation prior to elongation. Because of the methodology employed in this paper, trough fracture is entirely related to the 552-dam isohypses, not the vorticity pattern (which was unavailable for this step in the classification). A trough birth was classified as *closed low* if a trough was born when circling a closed 500-hPa low already detached from the main branch of the westerlies. Finally, *other* accommodated events not belonging to one of these five categories. [Doswell (1991) argued that classification schemes should have an unclassifiable category to avoid shoehorning unusual events into arbitrary categories.]

Second, the 500-hPa geostrophic thermal evolution (hereafter, thermal advection in this section) was classified as in Schultz and Doswell (1999): equivalent barotropic to cold advection (i.e., increasing cold advection), decreasing cold advection, weak advection or

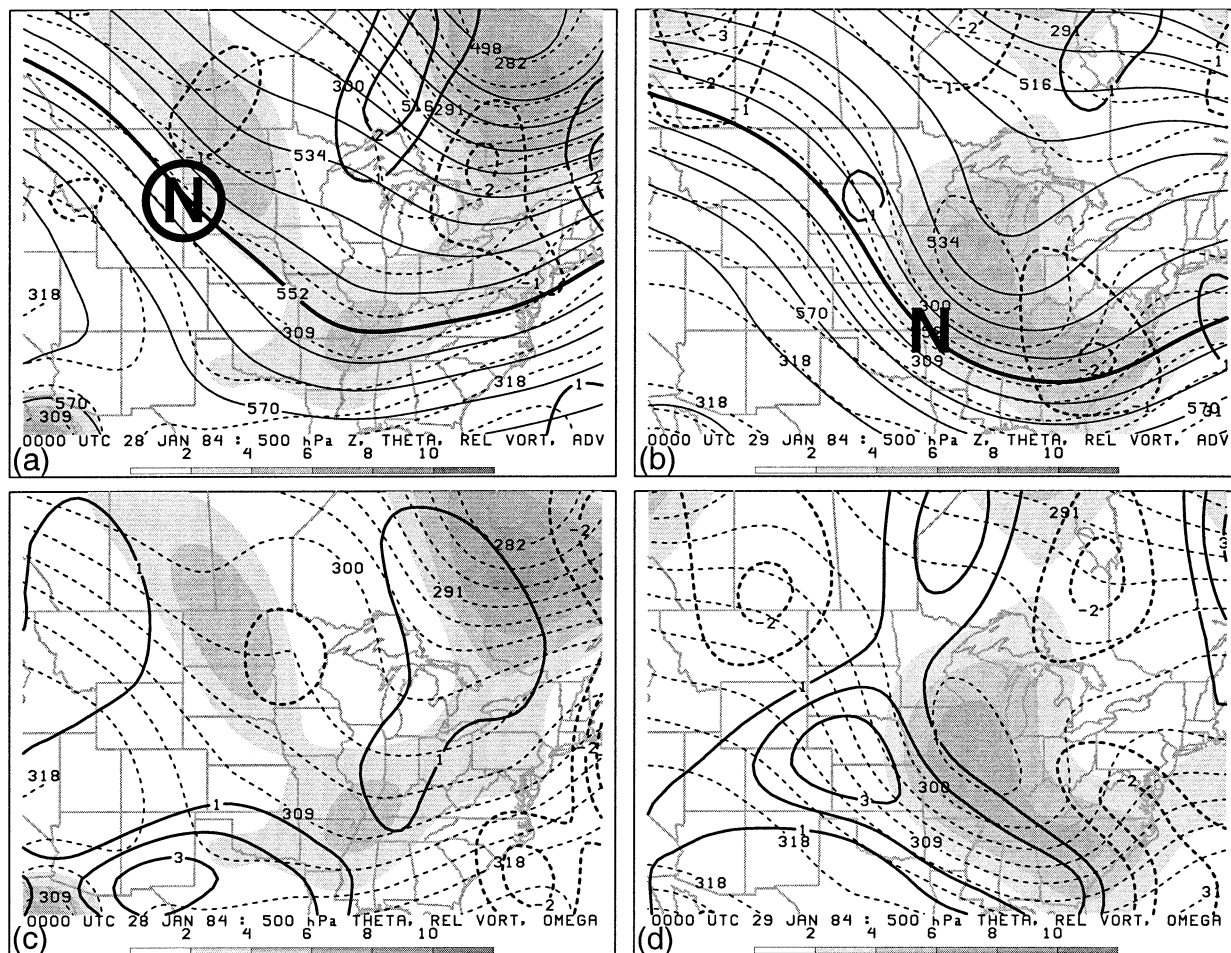


FIG. 1. Trough in diffluent flow: N represents the location of the trough, but, when encircled in (a), represents the trough birth in the notation of Sanders (1988). (a) The 500-hPa potential temperature advection by total horizontal wind (every $1 \times 10^{-4} \text{ K s}^{-1}$, contoured from -3 to $3 \times 10^{-4} \text{ K s}^{-1}$; thick solid lines represent warm advection and thick dashed lines represent cold advection), potential temperature (thin dashed lines every 3 K), geopotential height (thin solid lines every 6 dam; 552-dam isohypse bold), and relative vorticity of the total horizontal wind (10^{-5} s^{-1} , shaded according to scale) at 0000 UTC 28 Jan 1984. (b) As in (a) except at 0000 UTC 29 Jan 1984. (c) The 500-hPa omega [every 0.1 Pa s^{-1} from -0.6 to 0.4 Pa s^{-1} ; positive and zero (negative) values thick solid (dashed) and represent descent and no vertical motion (ascent), respectively], potential temperature (thin dashed lines every 3 K), and relative vorticity of the total horizontal wind (10^{-5} s^{-1} , shaded according to scale at bottom) at 0000 UTC 28 Jan 1984. (d) As in (c) except at 0000 UTC 29 Jan 1984.

equivalent barotropic, warm advection, or other. Geostrophic thermal advection was manually determined from the NMC 500-hPa maps for each event for a period no less than 24 h after trough birth. If the magnitude of the thermal gradient was nonnegligible and the angle between the isentropes and isohypses at and within about 1000 km downstream of, the location of the trough was less than about 5° for this 24-h period after trough birth, then the event was classified as *equivalent barotropic*. (Five degrees appeared to be about the lower limit for visually confirming geostrophic thermal advection from the NMC 500-hPa maps.) If, however, the thermal gradient subsequently evolved to produce increasing cyclonic rotation of the isentropes relative to the isohypses, then the event was classified as *increasing cold advection*. Typically, these cases where cyclonic rotation of the isentropes occurred were also associated

with increasing temperature gradient. Weakening of the thermal gradient or anticyclonic rotation of the isentropes implied *decreasing cold advection*. A thermal gradient that was weak or zero implied *weak advection*. If the isentropes were oriented relative to the isohypses so that warm advection occurred, then the event was classified as *warm advection*. Finally, if an event did not fit one of the four classifications above (e.g., the baroclinic zone evolved from cold advection to warm advection), then it was identified as *other*. These classifications are listed in Table 1. (One significant point is that although cold advection may not be occurring at the level of the upper-level front, if the trough is intensifying, cold advection should be decreasing with height below the trough, as per the quasigeostrophic height-tendency equation.)

While this classification scheme manually determines

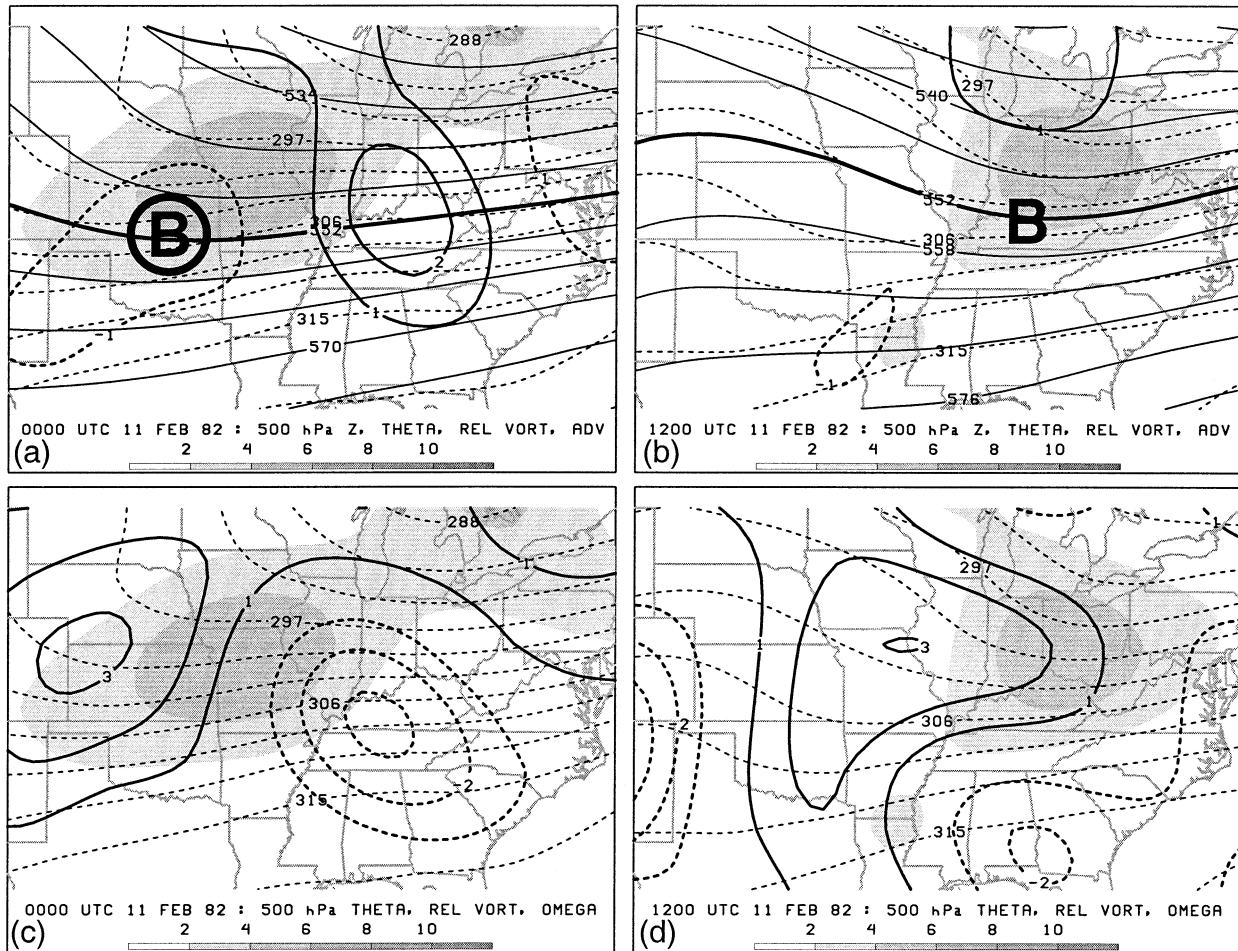


FIG. 2. As in Fig. 1 except for trough in confluent flow: (a), (c) 0000 UTC 11 Feb 1982 and (b), (d) 1200 UTC 11 Feb 1982. B represents the location of the trough, but, when encircled in (a), represents trough birth in the notation of Sanders (1988).

both the synoptic environment and thermal evolution, most of the events easily fit into one of the categories with little ambiguity, implying some robustness to this scheme. A manual approach was selected over an automated approach because it was felt that the tremendous effort involved in obtaining gridded data and computing diagnostics for 186 events would not change the results significantly. In addition, numerous subjective criteria about what constitute different synoptic environments and thermal evolutions would need to be determined, even for a so-called objective (i.e., automated) methodology (e.g., Kalkstein et al. 1987, p. 728). We choose, for these reasons, the more practical manual approach over automation.

Sections 2a–d illustrate the manual classification scheme with four examples: troughs in diffluent, confluent, and uniform flow, and trough fracture. The cases are illustrated with gridded analyses from the 2.5° latitude by 2.5° longitude NCEP–National Center for Atmospheric Research (NCAR) Reanalysis (Kalnay et al. 1996). These analyses are appropriate for the purposes of this study as their resolution is sufficient to illustrate

the synoptic-scale environment of the fronts, but not the mesoscale details of the fronts themselves. Since the troughs were classified according to the NMC 500-hPa maps, but are presented and diagnosed using the reanalysis data, some discrepancies may arise. Our experience suggests this will not affect the results of this study significantly. Ultimately, the NMC maps bear the actual rawinsonde data upon which the classification scheme was derived.

a. Trough in diffluent flow: 28 January 1984

Mobile trough N [in Sanders's (1988) naming convention] was born on 0000 UTC 28 January 1984 over the Dakotas (Fig. 1a), identified by a subtle depression in the 552-dam isohypse associated with a relative vorticity maximum to its northeast (Fig. 1a). The trough was born in northwesterly geostrophic flow with downstream diffluence associated with a predecessor vorticity maximum in the base of a longwave trough over the lower Mississippi River valley. Twelve hours later, the trough intensified, moved southeastward over Missouri/

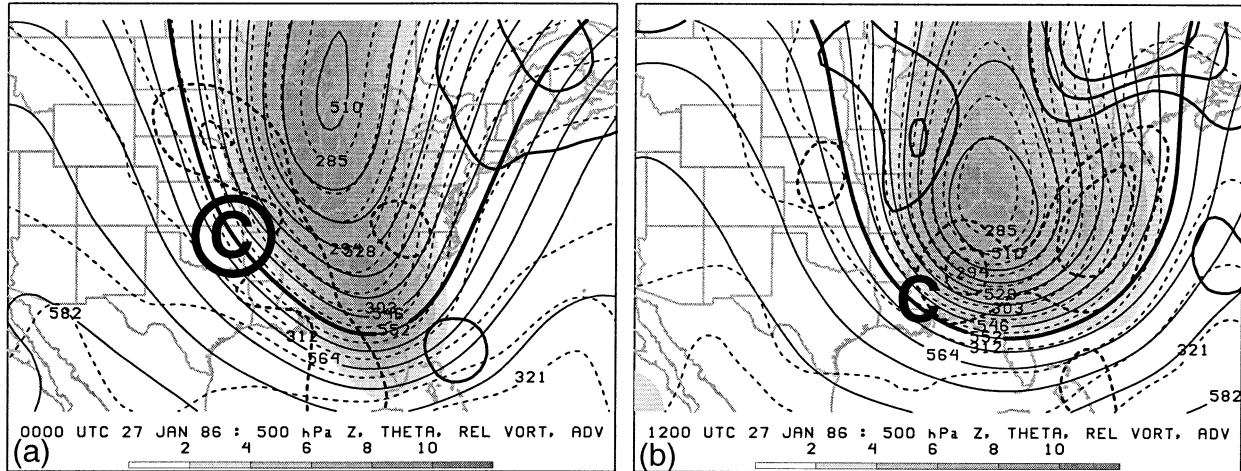


FIG. 3. Trough in uniform flow: C represents the location of the trough, but, when encircled in (a), represents trough birth in the notation of Sanders (1988). (a) The 500-hPa potential temperature advection by total horizontal (geostrophic and ageostrophic) wind (every 1×10^{-4} K s^{-1} , contoured from -3 to 3×10^{-4} K s^{-1} ; thick solid lines represent warm advection and thick dashed lines represent cold advection), potential temperature (thin dashed lines every 3 K), geopotential height (thin solid lines every 6 dam; 552-dam isohypse bold), and relative vorticity of the total horizontal wind (10^{-5} s^{-1} , shaded according to scale at bottom) at 0000 UTC 27 Jan 1986. (b) As in (a) except at 1200 UTC 27 Jan 1986.

Arkansas, and began to merge with the predecessor trough over the Carolinas (Fig. 1b), with increasing cold advection as the isentropes rotated cyclonically relative to the isohypses (cf. Figs. 1a,b). The along-flow length of the vorticity maximum decreased during this time. These characteristics are consistent with the compactor life cycle described by Lackmann et al. (1997) and discussed further by Schultz and Doswell (1999). Over the 24-h period, strong subsidence on the warm side of the intensifying vorticity maximum developed (cf. Figs. 1c,d). As shown in idealized modeling studies of upper-level frontogenesis (e.g., Shapiro 1981; Keyser and Pecnick 1985; Keyser et al. 1986; Reeder and Keyser 1988), this relationship between the descent and vorticity max-

imum aids further intensification of the trough/front system.

b. Trough in confluent flow: 11 February 1982

Mobile trough B was born on 0000 UTC 11 February 1982 over the central United States (Fig. 2a). Although the geostrophic flow was nearly westerly over the trough, the northwesterlies west of the trough over Nebraska and Wyoming led us to classify this event as a northwesterly flow trough birth (Fig. 2a). The stronger geostrophic flow over the eastern United States compared to that farther west implied that this trough was in confluent flow. Initially, relatively weak geostrophic

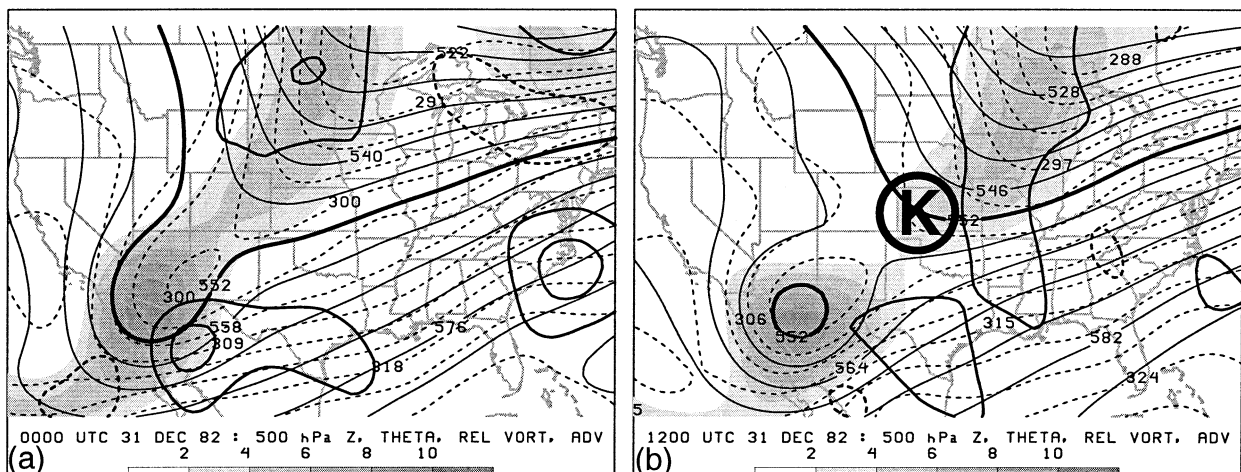


FIG. 4. As in Fig. 3 except for trough fracture: (a) 0000 UTC 31 Dec 1982; (b) 1200 UTC 31 Dec 1982. K represents the location of the trough, but, when encircled in (a), represents trough birth in the notation of Sanders (1988).

Table 1. Climatology of mobile-trough births in northwesterly flow, classified by the type of 500-hPa synoptic environment (columns) and evolution of the 500-hPa geostrophic thermal-advection pattern (rows). Entries in the table represent the number of events in each category from a 186-event dataset derived from the maps generated by Sanders (1988). Numbers in parentheses are percentages of column or row totals from 186 events.

Category	Diffluence	Uniform flow	Confluence	Trough fracture	Closed low	Other	Total
Increasing cold advection	19	20	1	7	1	1	49 (26%)
Decreasing cold advection	2	3	2	0	1	0	8 (4%)
Weak advection or equivalent barotropic	16	43	16	18	5	5	103 (55%)
Warm advection	4	7	1	0	0	0	12 (7%)
Other	3	2	2	2	3	2	14 (8%)
Total	44 (24%)	75 (40%)	22 (12%)	27 (15%)	10 (5%)	8 (4%)	186 (100%)

warm advection preceded the trough and relatively weak cold advection was centered on the location of the trough birth (Fig. 2a). Twelve hours later, the isentropes became more parallel to the isohypses (Fig. 2b); therefore, this event was classified as weak thermal advection/equivalent barotropic. Initially, descent was maximized on the upstream end of the vorticity maximum (Fig. 2c), but later, developed on the vorticity maximum (Fig. 2d).

c. Trough in uniform flow: 27 January 1986

Mobile trough C, identified with a vorticity maximum to its northeast, was born on 0000 UTC 27 January 1986 over Oklahoma (Fig. 3a). The trough was born in strong northwesterly geostrophic flow with relatively uniform geostrophic wind downstream. Twelve hours later, trough C moved into the base of a longwave trough over the southeast United States, with relatively weak cold advection as the isentropes were nearly parallel to the isohypses (Fig. 3b). This event was classified as weak thermal advection/equivalent barotropic.

d. Trough fracture: 1 January 1983

Mobile trough K was born on 1200 UTC 31 December 1982 (0000 UTC 1 January 1983, according to Sanders's daily 0000 UTC analyses). An elongating positively tilted trough extending from Arizona to North Dakota (Fig. 4a) fractured into a closed low over southern Arizona and mobile trough K in the westerlies over the central United States (Fig. 4b). (Although the vorticity had already fractured into two pieces by 0000 UTC 31 December, the troughs in the height field did not separate until 12 h later). One way to view trough fracturing is as an extreme example of the trough-in-diffuence category, as the strong deformation in the diffuent northerlies over the Wyoming area (Fig. 4a) acts to stretch an initial parent vorticity maximum into two offspring vorticity maxima. Later, trough K moved into downstream confluence, a natural result of the diffuent flow upstream. Temperature advection from the NMC maps remained relatively weak throughout this period (not shown), although the Reanalysis data suggests

warm advection (see the discussion regarding such discrepancies earlier in this section). A climatology of trough-fracture events and more case studies are found in Dean and Bosart (1996) and the references therein.

e. Climatology

The results of the 186-event climatology of 500-hPa trough genesis are shown in Table 1. The most frequent synoptic environment for trough genesis was uniform flow (40%, or 75 of 186 events), followed by diffuence (24%, or 44 events). Trough fracture and confluence were also relatively common (15% and 12%, respectively). Since the trough fracture events could be considered an extreme case of diffuence, the diffuence and trough-fracture cases, if combined, would be nearly as common as the uniform-flow category.

With respect to thermal advection, 55% (103 of 186 events) of trough births were associated with relatively small temperature advection at 500 hPa, whereas 26% (49 events) of trough births developed increasing cold advection (i.e., the equivalent-barotropic to cold-advection category). Other thermal advection patterns accounted for the remaining 19%. These results indicate that trough births typically are not associated with appreciable temperature advection at 500 hPa, but may develop cold advection later in their evolution.

Trough genesis was more likely to be associated with increasing 500-hPa cold advection when the flow was diffuent than otherwise. For example, 43% (19 of 44 events) of mobile troughs born in diffuent flow were associated with the equivalent-barotropic to cold-advection transition. In contrast, 27% (20 of 75 events) of mobile troughs born in uniform flow and 5% (1 of 22 events) of mobile troughs born in confluent flow were associated with this transition. Instead, a larger percentage of events was associated with weak advection as the flow categories became increasingly confluent (36% for diffuence, 57% for uniform flow, and 73% for confluence). Whereas diffuence tended to be associated with increasing cold advection, confluence tended to be not conducive to increasing cold advection. The reason for this relationship between confluence/dif-

fluence and thermal advection is explored in the next section.

3. Thermal-advection and frontogenesis diagnosis

To explore the thermal-advection patterns associated with mobile troughs/upper-level fronts and their relationship to the diffuence/confluence, we examine the terms in the thermal-advection tendency equation to explicitly show the three-dimensional processes that alter the thermal advection by the *total* horizontal wind, (d/dt) ($-\mathbf{V}_H \cdot \nabla_H \theta$):

$$\frac{d}{dt}(-\mathbf{V}_H \cdot \nabla_H \theta) = \underbrace{-\frac{d\mathbf{V}_H}{dt} \cdot \nabla_H \theta}_{\text{acceleration}} - \underbrace{\mathbf{V}_H \cdot \frac{d}{dt} \nabla_H \theta}_{\text{frontogenesis}}, \quad (1)$$

where

$$\begin{aligned} \frac{d}{dt} &= \frac{\partial}{\partial t} + u \frac{\partial}{\partial x} \Big|_p + v \frac{\partial}{\partial y} \Big|_p + \omega \frac{\partial}{\partial p}, \\ \mathbf{V}_H &= u\mathbf{i} + v\mathbf{j}, \\ \nabla_H &= \mathbf{i} \frac{\partial}{\partial x} \Big|_p + \mathbf{j} \frac{\partial}{\partial y} \Big|_p. \end{aligned}$$

The subscript p indicates differentiation on an isobaric surface and hereafter is implicit.

The two terms on the right-hand side of (1) represent the two ways to change the thermal advection: change the component of the wind speed perpendicular to the isentropes (the *acceleration term*) or change the temperature gradient across which the wind blows (the *frontogenesis term*). Rewriting the frictionless horizontal momentum equation (e.g., Bluestein 1992, p. 173),

$$\frac{d\mathbf{V}_H}{dt} = -f\mathbf{k} \times \mathbf{v} - \nabla_H \Phi, \quad (2)$$

$$= -f\mathbf{k} \times \mathbf{v}_{\text{ag}}, \quad (3)$$

and substituting the definition of vector frontogenesis (Keyser et al. 1988; Schultz and Doswell 1999) yields

$$\frac{d}{dt}(-\mathbf{V}_H \cdot \nabla_H \theta) = \underbrace{(f\mathbf{k} \times \mathbf{v}_{\text{ag}}) \cdot \nabla_H \theta}_{\text{acceleration}} - \underbrace{\mathbf{V}_H \cdot \mathbf{F}}_{\text{frontogenesis}}, \quad (4)$$

where f is the Coriolis parameter, \mathbf{v}_{ag} is the ageostrophic wind, and \mathbf{F} is the vector frontogenesis as defined by Schultz and Doswell (1999).

The vector frontogenesis of Schultz and Doswell (1999) is an extension of the formulation in Keyser et al. (1988) to include terms related to the vertical velocity. The formulation of Keyser et al. (1988) is a vector generalization of Petterssen's (1936) scalar definition of frontogenesis. Schultz and Doswell (1999) define vector frontogenesis, \mathbf{F} , as the Lagrangian rate

of change of the magnitude and direction of the *horizontal* potential temperature gradient due to the *three-dimensional* wind:

$$\mathbf{F} = \frac{d}{dt} \nabla_H \theta. \quad (5)$$

Resolving \mathbf{F} into natural coordinates (s, n) such that the s axis is locally tangent to an isentrope and the n axis points toward cold air (i.e., \mathbf{s} points in the same direction as the thermal wind), (5) becomes

$$\mathbf{F} = F_n \mathbf{n} + F_s \mathbf{s}, \quad (6)$$

where F_n is referred to as the scalar frontogenesis or the frontogenetical component and F_s is referred to as the rotational component (Keyser et al. 1988). Schultz and Doswell (1999) show that these terms can be written

$$F_n = \frac{1}{2} |\nabla_H \theta| (\nabla_H \cdot \mathbf{V}_H - E \cos 2\beta) - \frac{\partial \theta}{\partial p} \left(\frac{\partial \omega}{\partial n} \right), \quad (7a)$$

$$F_s = \frac{1}{2} |\nabla_H \theta| (\nabla_H \times \mathbf{V}_H - E \sin 2\beta) - \frac{\partial \theta}{\partial p} \left(\frac{\partial \omega}{\partial s} \right), \quad (7b)$$

where E is the resultant deformation and β is the local angle between an isentrope and the axis of dilatation measured in a counterclockwise direction. Equation (7a) for F_n comprises three terms related to divergence, deformation, and tilting, whereas (7b) for F_s comprises three terms related to relative vorticity, deformation, and tilting. As shown in Keyser et al. (1988), positive F_n implies frontolysis, whereas positive F_s implies cyclonic rotation of the isentropes.

Returning to the thermal-advection tendency equation (4) and inserting the frontogenetical and rotational components (6) yields

$$\begin{aligned} \frac{d}{dt}(-\mathbf{V}_H \cdot \nabla_H \theta) &= \underbrace{(f\mathbf{k} \times \mathbf{v}_{\text{ag}}) \cdot \nabla_H \theta}_{\text{acceleration}} - \underbrace{\mathbf{V}_H \cdot \mathbf{F}_n}_{F_n \text{ term}} - \underbrace{\mathbf{V}_H \cdot \mathbf{F}_s}_{F_s \text{ term}}. \quad (8) \end{aligned}$$

Thus, changing the temperature gradient can alter the thermal advection either by changing the magnitude of the thermal gradient (F_n term) or by rotating the thermal gradient (F_s term).

Consider a nearly straight upper-level front with the isentropes nearly parallel to the height contours (the equivalent-barotropic stage). In this case, if the ageostrophic flow is small or nearly parallel to the geostrophic flow, then F_n will be nearly perpendicular to \mathbf{V}_H and their dot product will be small. Consequently, the F_s term must dominate since F_s is parallel to \mathbf{V}_H . In this paper, we show that for the events described in this section, the F_s term in the temperature-advection tendency equation is the dominant term leading to the onset of cold advection in upper-level fronts in northwesterly flow. Next, we compute terms in these diagnostic equa-

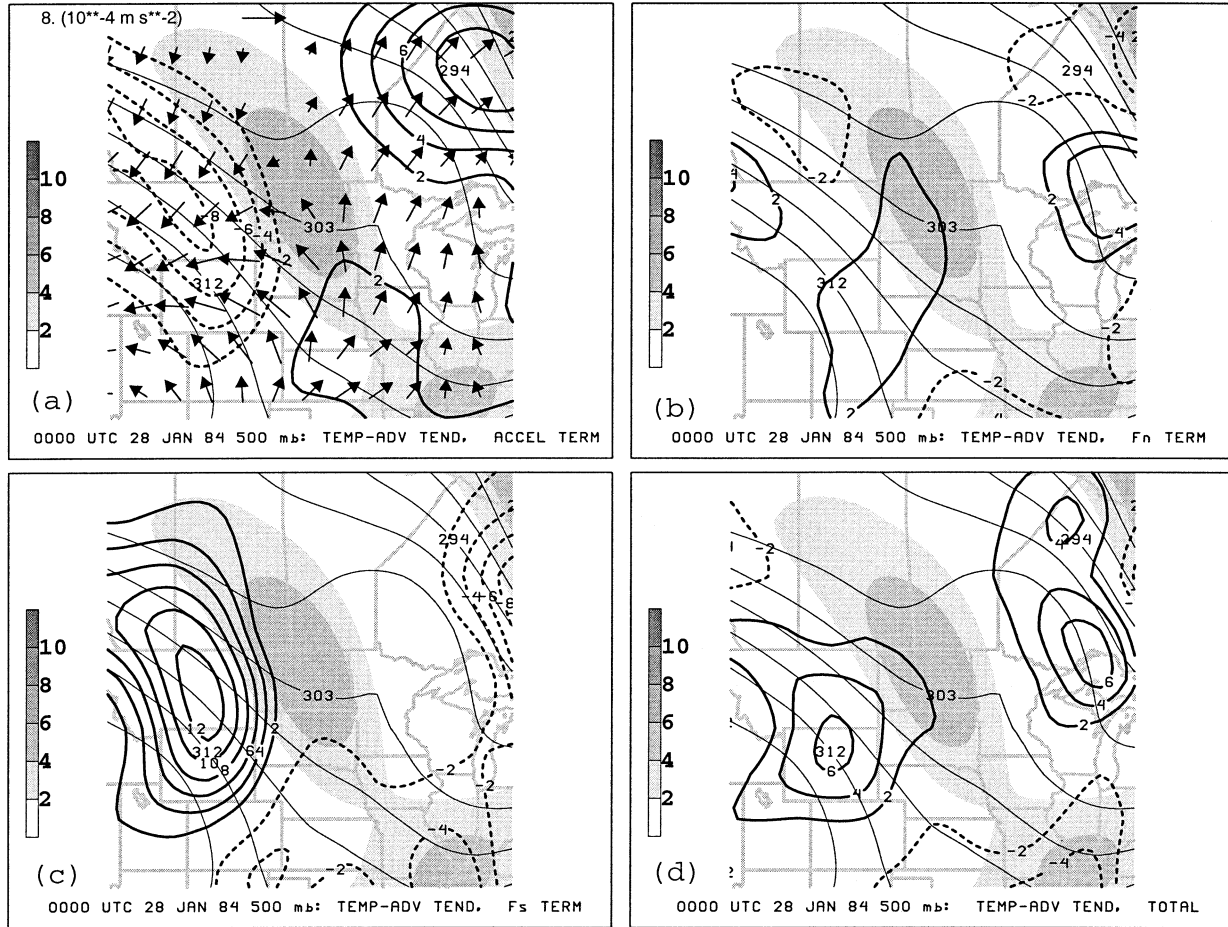


FIG. 5. Terms in the temperature-advection tendency equation (8) for the trough in diffidence at 0000 UTC 28 Jan 1984. (a) The 500-hPa relative vorticity of total horizontal wind (10^{-5} s^{-1} , shaded according to scale on the left side), potential temperature (thin solid lines every 3 K), acceleration vector (10^{-4} m s^{-2} , according to scale at top of panel), and acceleration term [every 2 K (24 h) $^{-2}$; positive (negative) values thick solid (dashed)]. (b) As in (a) except for the F_n term and no acceleration vectors. (c) As in (a) except for the F_s term and no acceleration vectors. (d) As in (a) except for total temperature-advection tendency and no acceleration vectors.

tions for the two cases of upper-level frontogenesis in diffidence and confluence described earlier.

a. Thermal-advection tendency

We begin our comparison by examining the terms in the thermal-advection tendency equation (8) for the mobile trough in diffidence from section 2a at 0000 UTC 28 January 1984 (Fig. 5) and for the mobile trough in confluence from section 2b at 0000 UTC 11 February 1982 (Fig. 6). Negative thermal-advection tendency represents decreasing warm advection or increasing cold advection, whereas positive thermal-advection tendency represents increasing warm advection or decreasing cold advection. The acceleration vector points upstream in decelerating diffluent flow and downstream in accelerating confluent flow. If the isentropes are nearly parallel to the flow, then the acceleration term, the dot product of the acceleration vector and the thermal gradient, will be small. Regions where the acceleration term is large

in such situations, thus, are associated with (a) thermal advection, (b) ageostrophic flow not associated with confluence/diffidence, or (c) both (a) and (b).

In the diffidence case (Fig. 5a), the acceleration term is large and negative in a region centered over Montana, a region of relatively small thermal advection west of the vorticity maximum associated with trough N (Fig. 1a). The strong acceleration toward higher heights (and higher temperatures) is associated with the supergeostrophic flow in the ridge in that location, implying negative thermal-advection tendency (Fig. 5a). On the downstream side of the vorticity maximum (e.g., Nebraska, Iowa), the acceleration term is small, confirming the unimportance of this term toward the thermal-advection tendencies in this region. In the confluence case (Fig. 6a), the acceleration term is relatively weak, but positive, everywhere.

In the diffidence case, the negative acceleration term is offset by a larger region of positive rotational frontogenesis (Fig. 5c). Thus, the total thermal-advection ten-

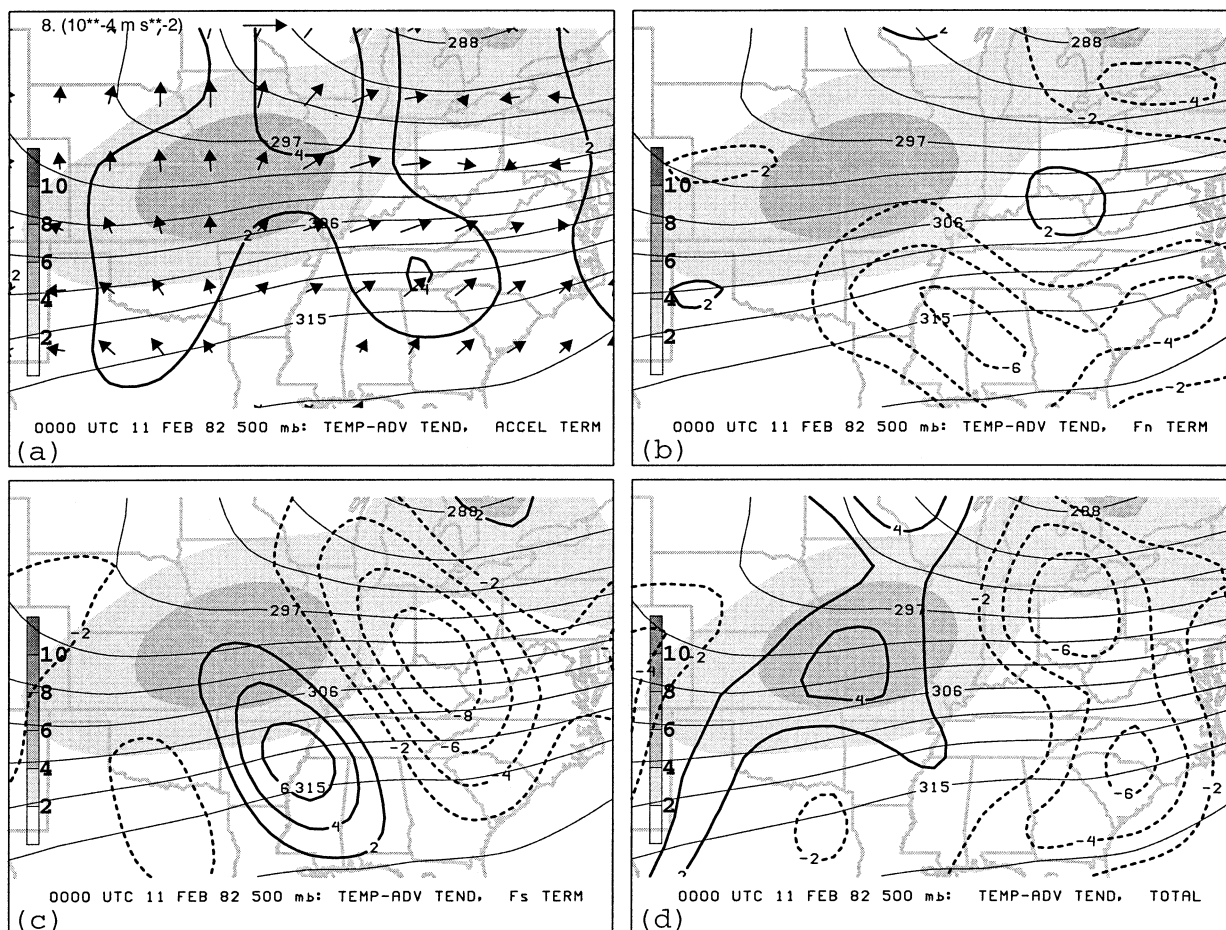


FIG. 6. As in Fig. 5 except for the trough in confluence at 0000 UTC 11 Feb 1982.

density (Fig. 5d) is positive west of the vorticity maximum. Indeed, the thermal advection in this region of the vorticity maximum evolves from relatively weak cold advection to relatively weak warm advection (cf. Figs. 1a,b). Downstream of the vorticity maximum over Missouri, however, the thermal-advection tendency is negative (Fig. 5d), indicating increasing cold advection, in agreement with the observations (Figs. 1a,b). The increasing cold advection in this region appears to be associated with the predecessor vorticity maximum over southeast Missouri.

Near the vorticity maximum in confluence, the rotational-frontogenesis term is large and dominates the total thermal-advection tendency in that region (cf. Figs. 6c,d). Over the vorticity maximum the rotational-frontogenesis term is positive whereas negative areas are found farther downstream, as in the diffluence case. Indeed, the observed thermal advection in that region changes from warm advection to relatively weak advection (negative thermal-advection tendency) (cf. Figs. 2a,b). Thus, the rotational-frontogenesis term favors increasing cold advection following the flow (i.e., from a Lagrangian perspective) in both the trough genesis

events in diffluence and confluence. To explore how the components of the frontogenesis vector act to change the thermal gradient, their contributions are explored in the next two sections.

b. Scalar frontogenesis: F_n

Examining the terms in (7a), the equation for the frontogenetical component of \mathbf{F} ($-F_n$), for the two cases of trough genesis (Figs. 7 and 8) shows the divergence term is small in both cases (Figs. 7a and 8a), as it was in the northwesterly flow event described in Schultz and Doswell (1999, their Figs. 8a and 9a). [We present $-F_n$ rather than F_n in Figs. 7 and 8 in order that regions of positive $-F_n$ represent regions of positive frontogenesis [Eq. (2.3a) in Keyser et al. (1988)].] The deformation term acts frontolytically in the diffluence case where isentropes are being stretched apart, but frontogenetically in the confluence case where isentropes are being brought together (cf. Figs. 7b and 8b). The main contribution to frontogenesis in the diffluence case comes from the tilting term (Fig. 7c), as in many other cases of upper-level frontogenesis in northwesterly flow (e.g.,

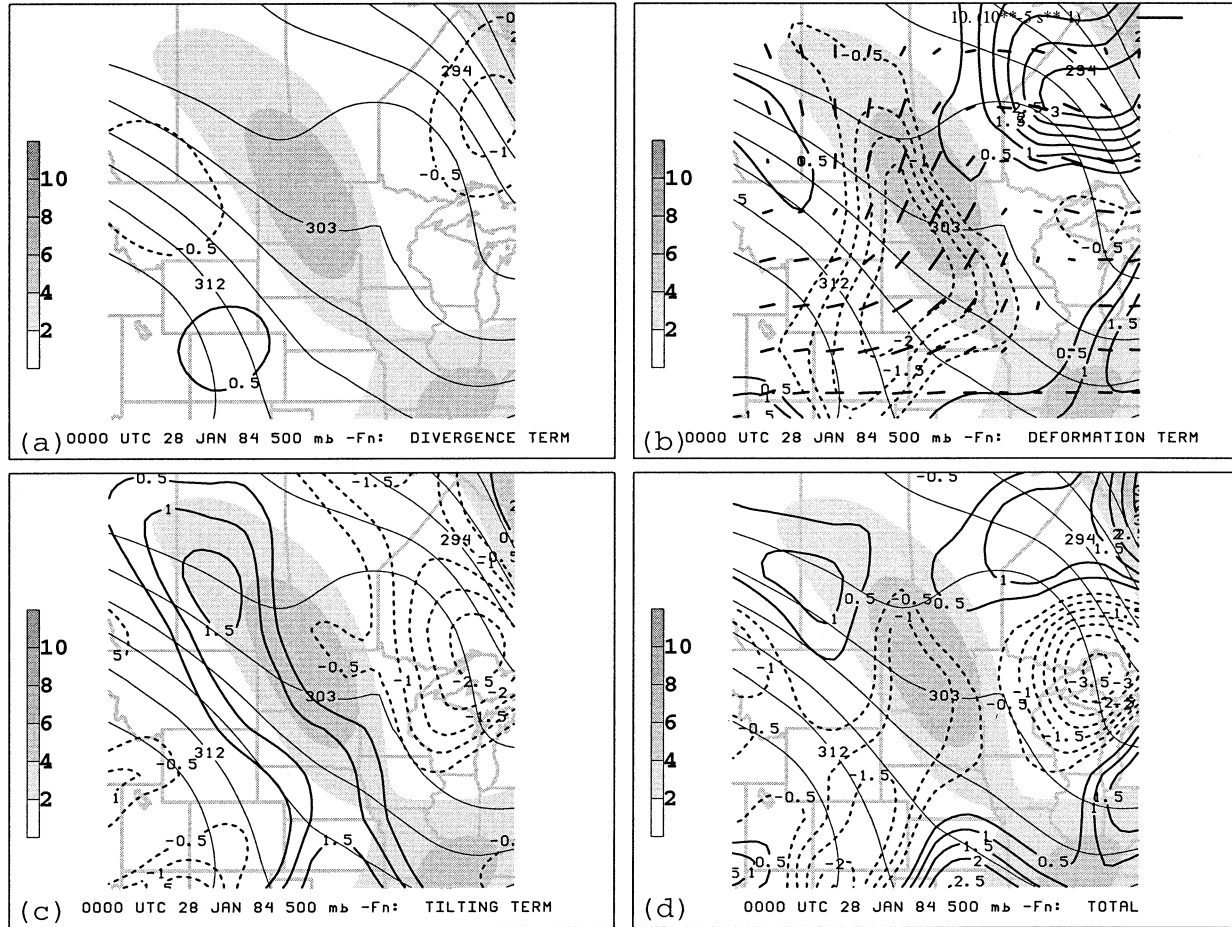


FIG. 7. Terms in the frontogenetical component of \mathbf{F} equation (7a) for the trough in diffuence at 0000 UTC 28 Jan 1984. (a) The 500-hPa relative vorticity of total horizontal wind (10^{-5} s^{-1} , shaded according to scale on the left side), potential temperature (thin solid lines every 3 K), and $-F_n$ divergence term [every $0.5 \times 10^{-10} \text{ K m}^{-1} \text{ s}^{-1}$; from -5 to $5 \times 10^{-10} \text{ K m}^{-1} \text{ s}^{-1}$; positive (negative) values thick solid (dashed)]. (b) As in (a) except for $-F_n$ deformation term and axes of dilatation of total horizontal wind [scaled according to line segment representing $10 \times 10^{-5} \text{ s}^{-1}$ in the upper right; separation between displayed axes is 2.5° (every grid point)]. (c) As in (a) except for $-F_n$ vertical tilting term. (d) As in (a) except for total $-F_n$.

Reed and Sanders 1953; Keyser and Shapiro 1986). Although the total frontogenesis was negative along much of the vorticity maximum (Fig. 7d), after 12 h, the tilting term dominated the deformation term (not shown), leading to an intensification of the upper-level front. In contrast, in the confluence case, the tilting term is frontolytic downstream of the vorticity maximum over Illinois, Indiana, and Ohio (Fig. 8c), so total frontogenesis is small, but positive (Fig. 8d).

c. Rotational component: F_s

We next examine the terms in (7b), the equation for the rotational component of \mathbf{F} (F_s). As in the northwesterly flow event in Schultz and Doswell (1999), the rotational component of \mathbf{F} for the diffuence case in the region of the vorticity maximum was dominated by the vorticity term (Fig. 9a), which was larger than either the deformation or tilting terms (cf. Figs. 9b,c). For the

confluence case, the vorticity and the tilting terms were of comparable magnitude with the deformation term smaller (cf. Figs. 10a–c). The tilting term was negative over the vorticity maximum in both cases, favoring increasing warm advection (Figs. 9c and 10c). Thus, the total rotational component was positive on the downstream side of the vorticity maximum in both cases (Figs. 9d and 10d). For the event in diffuence, positive F_s over Iowa, Nebraska, and Missouri (Figs. 9d) resulted in increasing cold advection (cf. Figs. 1a,b), as described by Schultz and Doswell (1999). In the confluence case, however, positive F_s over the Ohio River valley (Fig. 10d) resulted in decreasing warm advection (cf. Figs. 2a,b).

d. Rotation of isentropes in a Eulerian framework

Throughout the paper to this point, the diagnostics have been Lagrangian, meaning that the frontogenesis

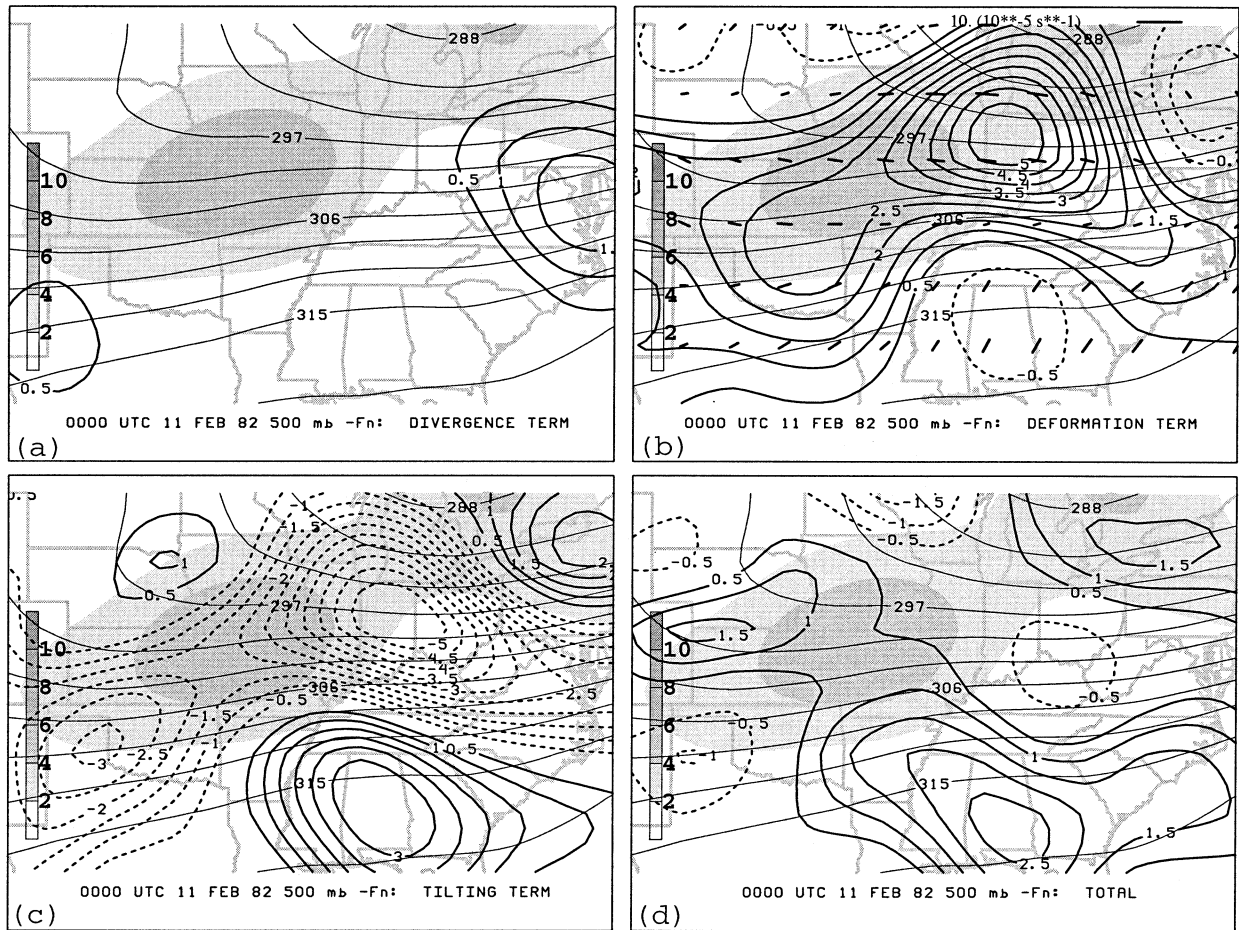


FIG. 8. As in Fig. 7 except for the trough in confluence at 0000 UTC 11 Feb 1982.

is measured relative to moving air parcels, not relative to the front or to a point on the earth's surface. Thus, at a given point, even fronts that are weakening may experience positive Lagrangian frontogenesis. To account for advection, we derive the Eulerian formulation of F_s , which diagnoses the causes of thermal-advection changes.

Keyser et al. (1988, p. 764) present the following expression:

$$F_s = |\nabla_H \theta| \frac{d\alpha}{dt}, \tag{9}$$

where α is the orientation of the isentrope, the angle between the positive x axis and an arbitrary isentrope on an isobaric surface, measured in a counterclockwise direction. Expanding $d\alpha/dt$,

$$\frac{d\alpha}{dt} = \frac{\partial \alpha}{\partial t} + u \frac{\partial \alpha}{\partial x} + v \frac{\partial \alpha}{\partial y} + \omega \frac{\partial \alpha}{\partial p}. \tag{10}$$

Solving for $\partial \alpha / \partial t$,

$$\frac{\partial \alpha}{\partial t} = \underbrace{|\nabla_H \theta|^{-1} F_s}_{\text{normalized rotational component of } \mathbf{F}} - \underbrace{u \frac{\partial \alpha}{\partial x} + v \frac{\partial \alpha}{\partial y}}_{\text{horizontal advection}} - \underbrace{\omega \frac{\partial \alpha}{\partial p}}_{\text{vertical advection}}. \tag{11}$$

Therefore, the Eulerian formulation (11) can be used to evaluate the three factors that cause the rotation of the isentropes at a point: the normalized rotational component of \mathbf{F} (normalized F_s) [composed of vorticity, deformation, and tilting terms by (7b)], horizontal advection of α , and vertical advection of α . Since advection can only move around isentrope angle α but cannot increase α , normalized rotational frontogenesis is the only term that can diagnose the change of the isentrope angle in a Lagrangian sense. Therefore, either vertical advection or normalized rotational frontogenesis must be associated with the changing angle of the isentropes on a constant-pressure surface that leads to increasing cold advection.

In the diffluence case, the local rotation of the isentropes was dominated by the large positive $\partial \alpha / \partial t$ (cyclonic rotation) at the downstream end of the vorticity

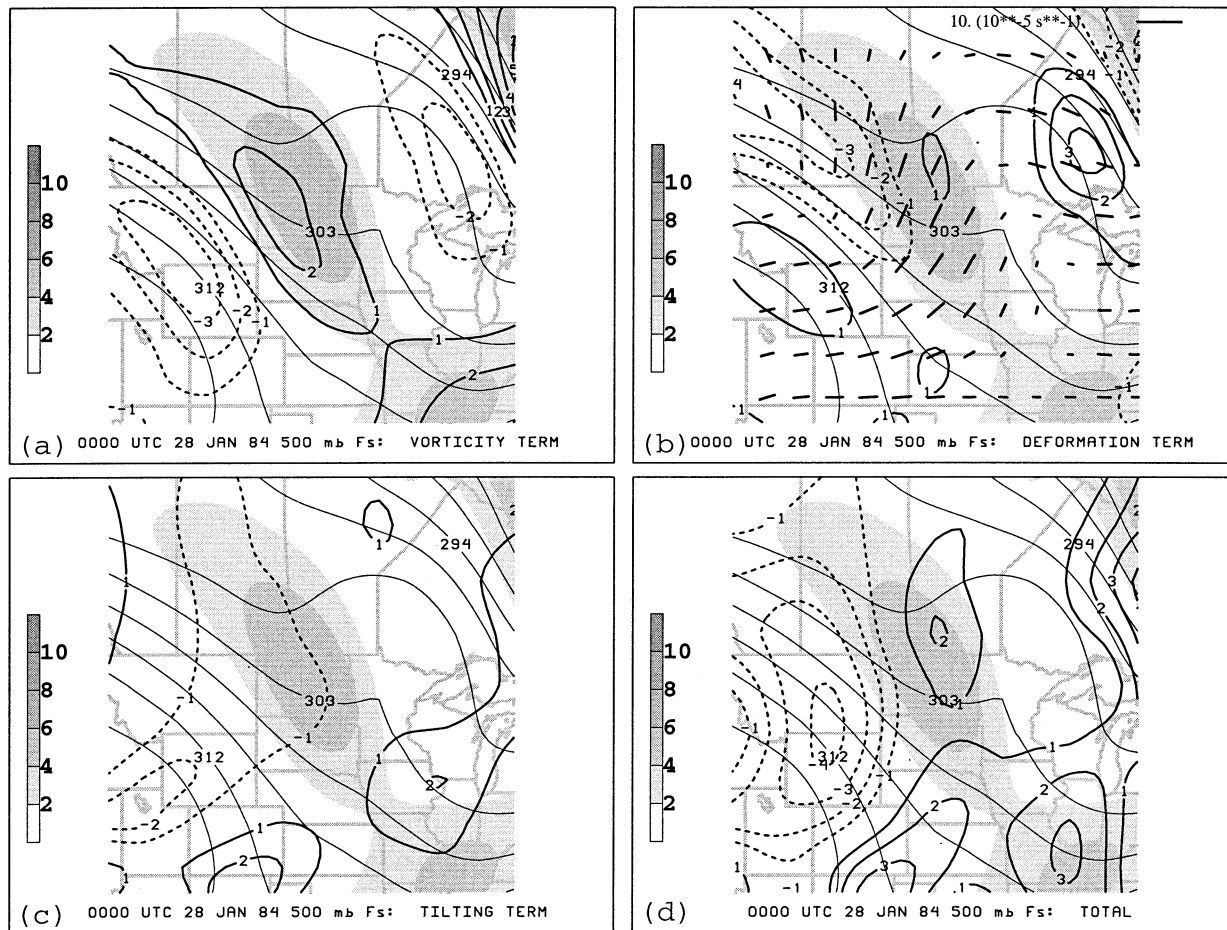


FIG. 9. Terms in the rotational component of \mathbf{F} equation (7b) for the trough in diffuence at 0000 UTC 28 Jan 1984. (a) The 500-hPa relative vorticity of total horizontal wind (10^{-5} s^{-1} , shaded according to scale on the left side), potential temperature (thin solid lines every 3 K), and F_s vorticity term [every $10^{-10} \text{ K m}^{-1} \text{ s}^{-1}$; positive (negative) values thick solid (dashed)]. (b) As in (a) except for F_s deformation term and axes of dilatation of total horizontal wind [scaled according to line segment representing $10 \times 10^{-5} \text{ s}^{-1}$ in upper right; separation between displayed axes of dilatation is 2.5° (every grid point)]. (c) As in (a) except for F_s vertical tilting term. (d) As in (a) except for total F_s .

maximum, with a smaller region of negative $\partial\alpha/\partial t$ (anticyclonic rotation) at the upstream end (Fig. 11d). Because of the large horizontal gradient of α over Minnesota and southern Canada, horizontal advection plays a large role (Fig. 11b). In the diffuence case, the normalized rotational component and horizontal advection were important to producing cyclonic rotation of the isentropes (Figs. 11a,b), favoring the development of the cold advection at the downstream side. In both cases, the vertical advection of α was negligible (Figs. 11c and 12c) and thus cannot be responsible for the onset of cold advection along the upper-level front. Instead, the increasing cold advection in the diffuence case was caused by the vorticity term of F_s . Thus, these diagnostics for this event provide support for the results from the climatology in which trough births in diffuence favor increasing cold advection.

In the confluent-flow case, the normalized rotational frontogenesis is small compared to the horizontal advection term (cf. Figs. 12a,b), such that the total isen-

trope rotation is dominated by anticyclonic rotation at the upstream end of the vorticity maximum (Fig. 12d). This pattern tends to reduce the cold advection, in contrast to the event in diffuence flow, where the cyclonic rotation was maximized at the downstream end of the vorticity maximum, which led to increasing cold advection. Thus, these diagnostics for this event demonstrate why the majority of confluent-flow cases from the climatology did not produce strong thermal advection.

e. Differences between frontogenesis in diffuence and confluence flow

Summarizing the results of the diagnostics in this section, we find the following for these two cases of upper-level frontogenesis in northwesterly flow.

- Positive 500-hPa rotational frontogenesis is found downstream of the vorticity maximum in both cases.
- The primary term leading to 500-hPa frontogenesis

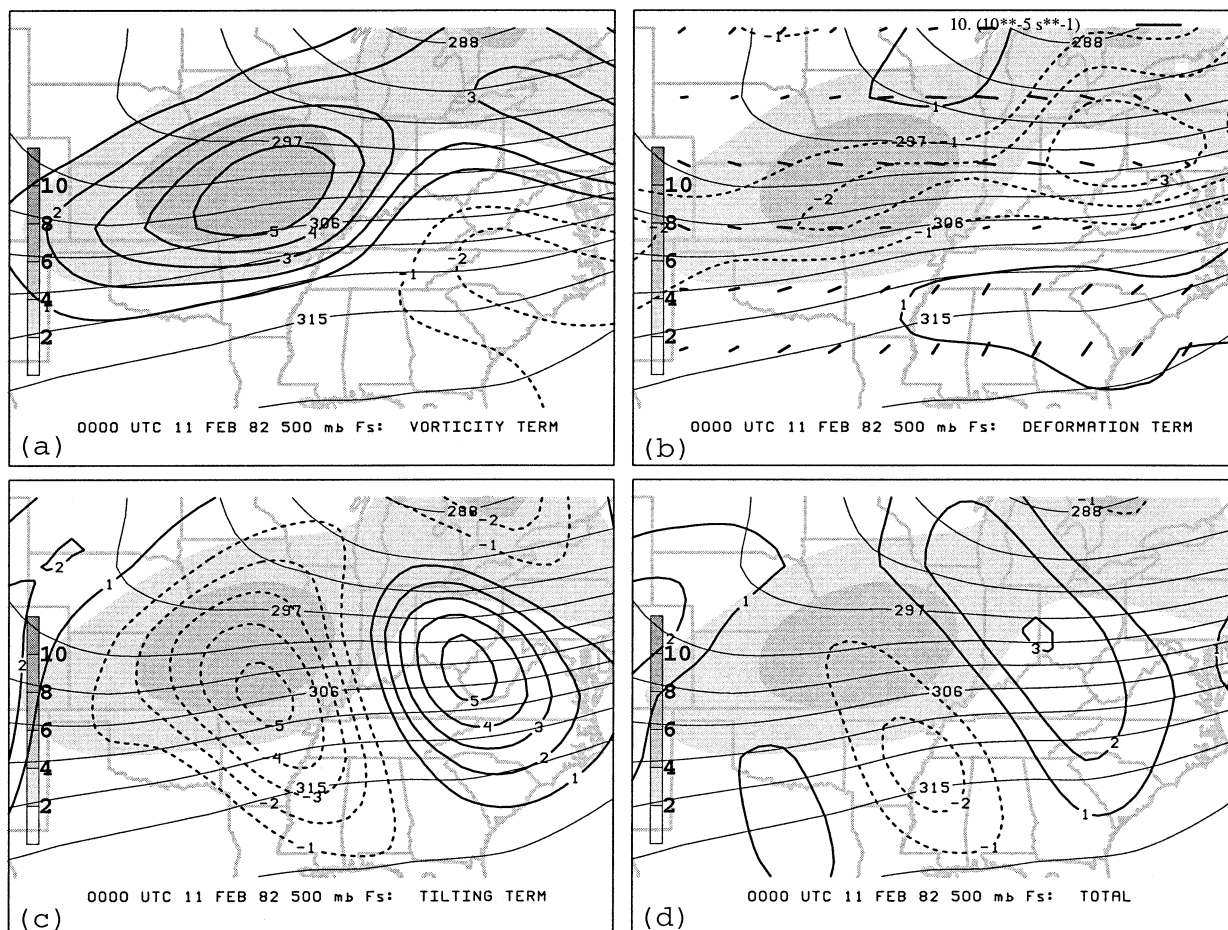


FIG. 10. As in Fig. 9 except for the trough in confluence at 0000 UTC 11 Feb 1982.

($-F_n$) is tilting in the diffluence case and deformation in the confluence case.

- In both diffluence and confluence cases, the vorticity term in the rotational frontogenesis equation is responsible for rotating the isentropes into a position favoring increasing 500-hPa cold advection (or decreasing 500-hPa warm advection) downstream of the vorticity maximum.
- In both cases, the tilting term in the rotational frontogenesis equation acts to rotate the isentropes in the region of the 500-hPa vorticity maximum toward warm advection, not cold advection.
- The Eulerian formulation of F_s shows that strong rotation of the isentropes downstream of the 500-hPa vorticity maximum is favored in the diffluence case, whereas rotation of the isentropes is suppressed on the downstream side of the 500-hPa vorticity maximum in the confluence case. This result supports that from the climatology in which events in diffluent flow tend to be associated with increasing 500-hPa cold advection whereas those events in confluent flow tend to be associated with suppressing 500-hPa cold advection.

This diagnosis suggests the following reasoning. In diffluent flow, the vorticity associated with the incipient trough is compacted into a more circular shape and intensifies. The potent vorticity maximum leads to robust isentropes rotation. In confluent flow, however, the vorticity is deformed into an elongated maximum, inhibiting both strong isentropes rotation and increasing cold advection.

4. Discussion

Previous studies of upper-level frontogenesis have focused on confluence and cold advection in northwesterly flow as important to intensification of the front. In particular, the Shapiro effect (both confluence and cold advection acting to enhance upper-level frontogenesis) is argued to lead to intensification. As seen from the climatology in Table 1, however, not all 500-hPa trough births are associated with confluence or cold advection. Although upper-level frontogenesis may be most efficient in the presence of both confluence and cold advection, neither appears to be required for many mobile trough births (Table 1). While two-dimensional simu-

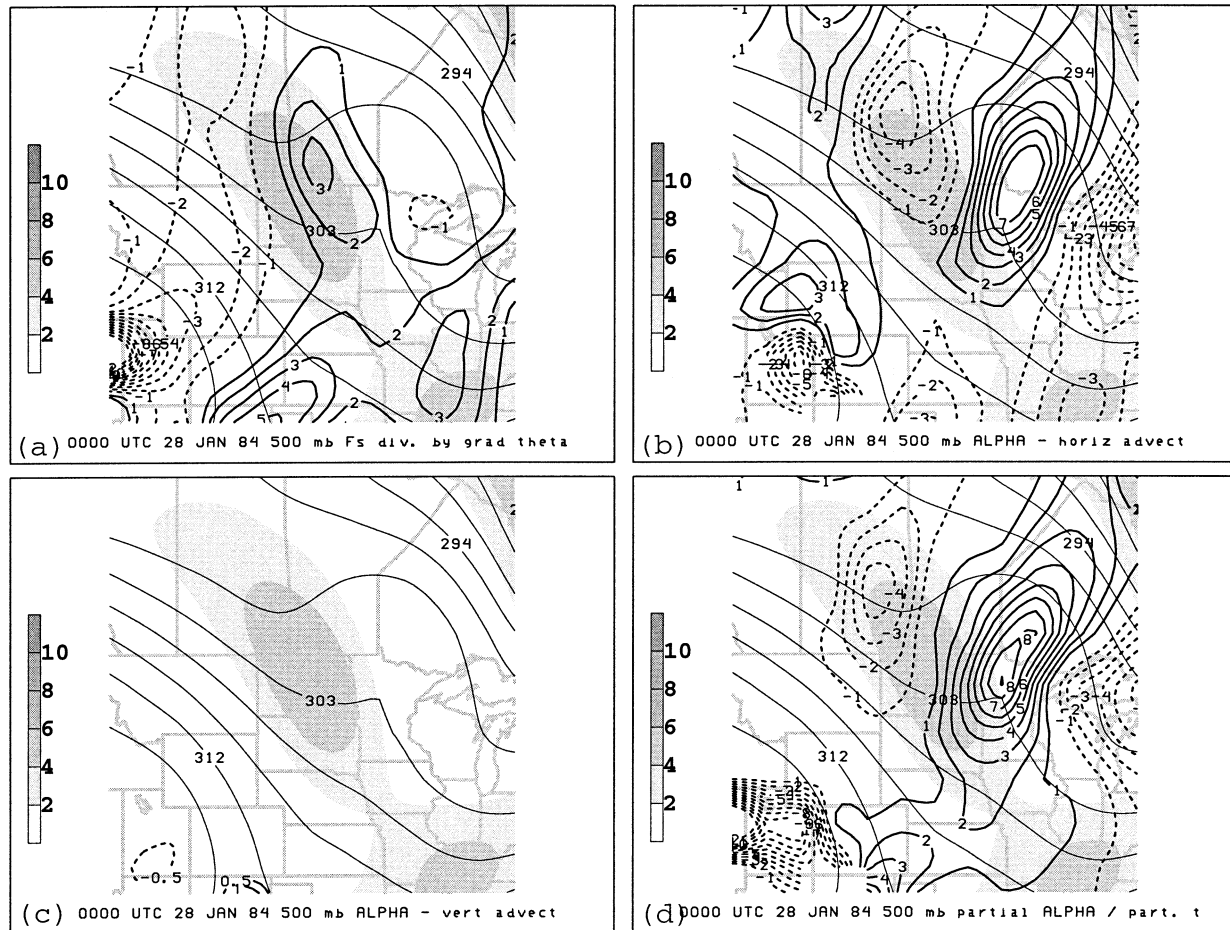


FIG. 11. Terms in the Eulerian rate of rotation equation (11) for the trough in diffluence at 0000 UTC 28 Jan 1984. (a) The 500-hPa relative vorticity of total horizontal wind (10^{-5} s^{-1} , shaded according to scale on the left side), potential temperature (thin solid lines every 3 K), and normalized F_s [every 10^{-5} s^{-1} from -10 to $14 \times 10^{-5} \text{ s}^{-1}$; positive (negative) values thick solid (dashed)]. (b) As in (a) except for horizontal advection of α . (c) As in (a) except for vertical advection of α (contoured $-1, -0.5, 0.5,$ and $1 \times 10^{-5} \text{ s}^{-1}$). (d) As in (a) except for $\partial\alpha/\partial t$.

lations of upper-level frontogenesis show that confluence and cold advection lead to more intense frontogenesis, confluence alone, in the absence of cold advection, is sufficient to produce upper-level frontogenesis (e.g., Keyser and Pecnick 1985; Reeder and Keyser 1988). Results from the climatology described in this paper, as well as earlier work by Sanders et al. (1991, 1364–1365) and Schultz and Doswell (1999, Table 1), support this modeling result.

For example, the climatology suggests that 500-hPa cold advection is more likely to develop as the mobile troughs move into diffluence. Diffluent flow favors both the intensification of the front through tilting of isentropes through the frontogenetical component of \mathbf{F} (F_n) and the onset of cold advection through the rotational component (F_s). The diffluence acts in two ways to intensify the vorticity maximum. First, the diffluence rotates the isentropes relative to the isohypses, producing cold advection. Through the quasigeostrophic height-tendency equation, if the cold advection were

decreasing with height, height falls would intensify the trough. Alternatively, this could be viewed as cold advection forcing descent through the quasigeostrophic omega equation. This descent is a maximum somewhere in the mid- to upper troposphere. Below the maximum descent there is divergence, anticyclonic vorticity increases, and height rises. Above it, there is convergence, cyclonic vorticity increases, and height falls (i.e., upper-level trough intensification). Second, the diffluence compacts the vorticity maximum, making it a more potent cyclogenetic precursor (e.g., Farrell 1989; Lefevre and Nielsen-Gammon 1998; Lackmann et al. 1997, 1999). Lackmann et al. (1999) showed that the increase in eddy kinetic energy in a jet streak located upstream of a developing trough was due to a Reynolds stress mechanism, a barotropic process that converts the kinetic energy of the jet stream to kinetic energy of the jet streak associated with the mobile trough. The associated transverse divergent circulations then favor upper-level frontogenesis and amplification of the vorticity

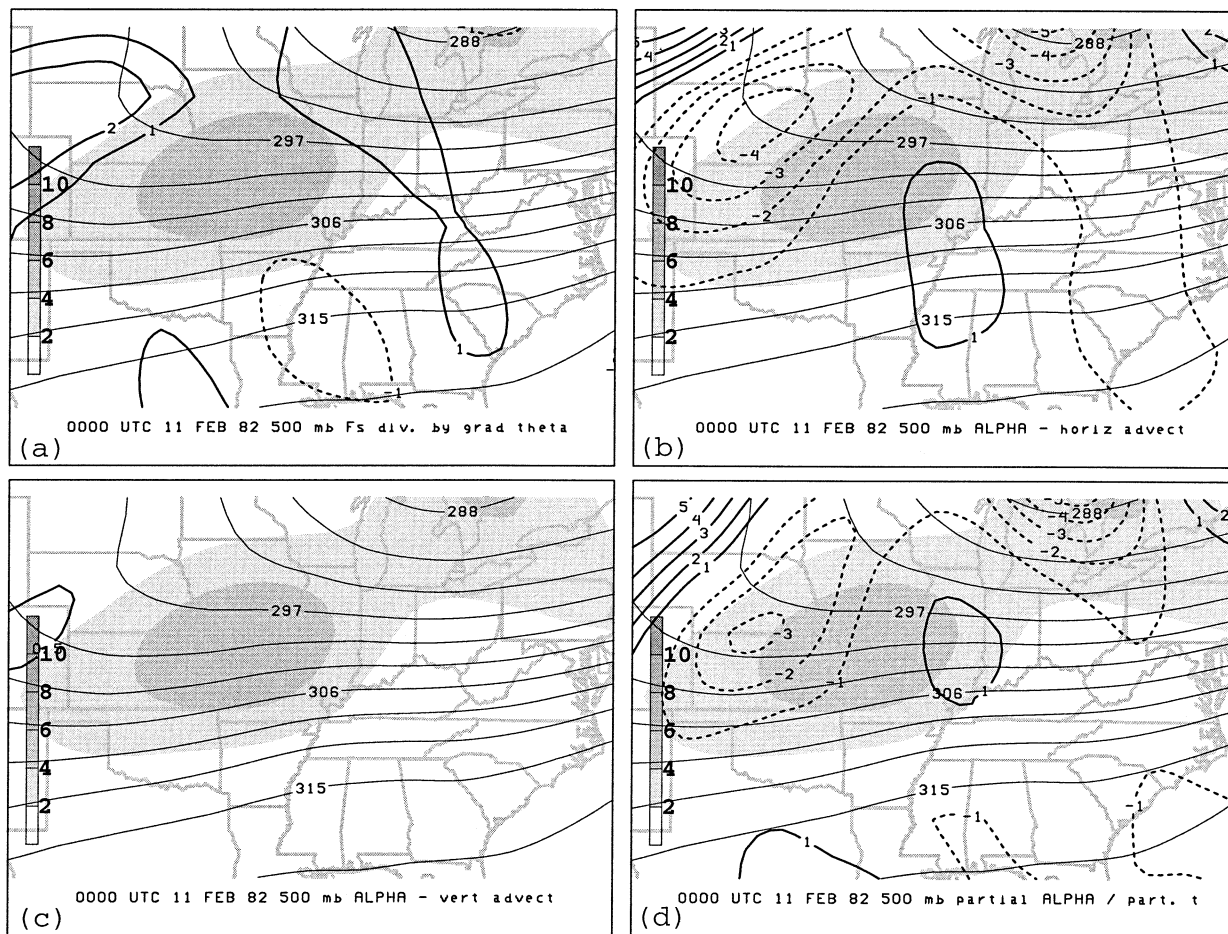


FIG. 12. As in Fig. 11 except for the trough in confluence at 0000 UTC 11 Feb 1982.

maximum. Since the Reynolds stress term is composed solely of expressions related to the horizontal wind (Lackmann et al. 1999, appendix), we infer that thermal advection, while perhaps enhancing upper-level frontogenesis, would not appear to be crucial to mobile trough intensification. Indeed, Farrell (1989) showed that zonally elongated disturbances in a barotropic model could intensify if they moved into diffluent flow, analogous to the compaction process studied by Lackmann et al. (1997, 1999). Sanders (1988, p. 2639) also hypothesized that barotropic processes may be acting in these situations.

Another example of trough genesis where thermal advectons appear to be unimportant is the idealized simulations of Rotunno et al. (1994). Rotunno et al. (1994) argue that in the early stages of upper-level frontogenesis, when thermal advection is small, diffluence on the cold-air side of the frontal zone and confluence on the warm-air side induces frontogenetical tilting that favors increasing cold advection and trough amplification. Thus, trough amplification apparently can occur in the absence of the frontogenetical feedback provided by the Shapiro effect (Keyser 1999, 254–255). More-

over, Wandishin et al. (2000, p. 3935) argued that the vertical circulations that enhance tropopause folding do so along the length of the front and are not exclusively tied to regions of cold advection. The apparent similarity of the association between alongfront cold advection, subsidence on the warm side of the front, and frontal intensification, therefore, may arise from a variety of different mechanisms. This collective evidence suggests that barotropic processes can be responsible for the generation and intensification of mobile troughs.

5. Summary

The purpose of this study was to explore the variety of synoptic environments and thermal-advection patterns associated with the birth of 500-hPa mobile troughs in northwesterly flow. A climatology derived from the Sanders (1988) dataset identified 186 mobile trough births in 500-hPa northwesterly flow over North America during 10.5 cold seasons. The 500-hPa synoptic environment in which each of these 186 events was born was classified: 40% in uniform flow, 24% in diffluent flow, 11% in confluent flow, and the remaining

25% in one of three other categories. The 500-hPa thermal-advection pattern associated with each mobile trough was also categorized: 55% had weak advection, 26% had increasing cold advection, and the remaining 19% were in one of three other categories. Mobile troughs in diffluent flow were more likely to develop increasing cold advection, whereas troughs in confluent flow were more likely to be associated with weak advection and inhibit increasing cold advection.

Two case studies were examined to understand the kinematic processes acting to cause the 500-hPa thermal advectons observed in the climatology. One case was a mobile trough born in diffluence, whereas the other case was a mobile trough born in confluence. Specifically, the vector frontogenesis function, as generalized by Schultz and Doswell (1999), was employed to compute the effects of the three-dimensional wind on the Lagrangian rate of change of the magnitude and direction of the horizontal potential temperature gradient associated with the mobile troughs. The most important processes leading to intensification of the temperature gradient were tilting for the case in diffluence and deformation for the case in confluence. The rotational component of vector frontogenesis can be viewed as a measure of the flow's effect on the relative orientation of the isentropes and thus, indirectly, a measure of the changes in the thermal-advection pattern. For the case in diffluence, forcing for isentrope rotation was primarily cyclonic and located downstream of the trough, which would explain the prevalence of increasing cold advection among mobile trough births in diffluence in the climatology. By contrast, in the confluent case, forcing for isentrope rotation was primarily anticyclonic and located upstream of the trough, which would offset the cyclonic effect due to the vorticity and explain the prevalence for weak thermal advection (or inhibition of cold advection) among mobile trough births in confluence in the climatology.

This study, however, does not quantify the Shapiro effect (the combined effect of confluence and cold advection on upper-level frontogenesis) in a large number of cases. A more thorough climatology would need to be performed. As noted by Keyser (1999), confirmation of the Shapiro effect in observational studies of upper-level fronts remains undone. Nevertheless, this study has implications for the two-dimensional idealized models that have been published previously, showing that mobile trough births can occur in situations that are less than optimal for intensification (e.g., in the absence of confluence and cold advection). Mobile trough genesis and upper-level frontogenesis can occur in a variety of environments and with a variety of evolutions (see also Lackmann et al. 1997, Table 1), such that simple conceptual models (e.g., Shapiro 1982; Schultz and Doswell 1999) do not fully explain the variety of these features in the real atmosphere. Hopefully, this study will serve as possible guidance toward increasing the sophistication of three-dimensional idealized models of baroclinic

waves through more realistic depictions of background flows and initial conditions for such disturbances, allowing for greater realism and variety in the simulated structures and evolutions.

Acknowledgments. We have benefited considerably from discussions with and comments from Charles Doswell, David Dowell, Gregory Hakim, Daniel Keyser, John Knox, Gary Lackmann, Harald Richter, Richard Rotunno, James Steenburgh, Matthew Wandishin, and the anonymous reviewers. The Storm Prediction Center graciously provided access to their microfilm archives of NMC maps.

REFERENCES

- Bluestein, H. B., 1992: *Principles of Kinematics and Dynamics*. Vol. I. *Synoptic-Dynamic Meteorology in Midlatitudes*, Oxford University Press, 431 pp.
- , 1993: *Observations and Theory of Weather Systems*. Vol. II. *Synoptic-Dynamic Meteorology in Midlatitudes*, Oxford University Press, 594 pp.
- Dean, D. B., and L. F. Bosart, 1996: Northern Hemisphere 500-hPa trough merger and fracture: A climatology and case study. *Mon. Wea. Rev.*, **124**, 2644–2671; Corrigendum, **125**, 661.
- Doswell, C. A., III, 1991: Comments on mesoscale convective patterns of the southern high plains. *Bull. Amer. Meteor. Soc.*, **72**, 389–390.
- Farrell, B. F., 1989: Transient development in confluent and diffluent flow. *J. Atmos. Sci.*, **46**, 3279–3288.
- Hakim, G. J., 2000: Climatology of coherent structures on the extratropical tropopause. *Mon. Wea. Rev.*, **128**, 385–406.
- Kalkstein, L. S., G. Tan, and J. A. Skindlov, 1987: An evaluation of three clustering procedures for use in synoptic climatological classification. *J. Climate Appl. Meteor.*, **26**, 717–730.
- Kalnay, E., and Coauthors, 1996: The NCEP/NCAR 40-Year Reanalysis Project. *Bull. Amer. Meteor. Soc.*, **77**, 437–471.
- Karoly, D. J., and B. J. Hoskins, 1982: Three dimensional propagation of planetary waves. *J. Meteor. Soc. Japan*, **60**, 109–123.
- Keyser, D., 1999: On the representation and diagnosis of frontal circulations in two and three dimensions. *The Life Cycles of Extratropical Cyclones*, M. A. Shapiro and S. Grønås, Eds., Amer. Meteor. Soc., 239–264.
- , and M. J. Pecnick, 1985: A two-dimensional primitive equation model of frontogenesis forced by confluence and horizontal shear. *J. Atmos. Sci.*, **42**, 1259–1282.
- , and M. A. Shapiro, 1986: A review of the structure and dynamics of upper-level frontal zones. *Mon. Wea. Rev.*, **114**, 452–499.
- , M. J. Pecnick, and M. A. Shapiro, 1986: Diagnosis of the role of vertical deformation in a two-dimensional primitive equation model of upper-level frontogenesis. *J. Atmos. Sci.*, **43**, 839–850.
- , M. J. Reeder, and R. J. Reed, 1988: A generalization of Petterssen's frontogenesis function and its relation to the forcing of vertical motion. *Mon. Wea. Rev.*, **116**, 762–780.
- Lackmann, G. M., D. Keyser, and L. F. Bosart, 1997: A characteristic life cycle of upper-tropospheric cyclogenetic precursors during the Experiment on Rapidly Intensifying Cyclones over the Atlantic (ERICA). *Mon. Wea. Rev.*, **125**, 2729–2758.
- , —, and —, 1999: Energetics of an intensifying jet streak during the Experiment on Rapidly Intensifying Cyclones over the Atlantic (ERICA). *Mon. Wea. Rev.*, **127**, 2777–2795.
- Lefevre, R. J., and J. W. Nielsen-Gammon, 1995: An objective climatology of mobile troughs in the Northern Hemisphere. *Tellus*, **47A**, 638–655.
- Mass, C. F., H. J. Edmon, H. J. Friedman, N. R. Cheney, and E. E. Recker, 1987: The use of compact discs for the storage of large

- meteorological and oceanographic data sets. *Bull. Amer. Meteor. Soc.*, **68**, 1556–1558.
- Nielsen-Gammon, J. W., 1995: Dynamical conceptual models of upper-level mobile trough formation: Comparison and application. *Tellus*, **47A**, 705–721.
- , and R. J. Lefevre, 1996: Piecewise tendency diagnosis of dynamical processes governing the development of an upper-tropospheric mobile trough. *J. Atmos. Sci.*, **53**, 3120–3142.
- Orlanski, I., and J. P. Sheldon, 1995: Stages in the energetics of baroclinic systems. *Tellus*, **47A**, 605–628.
- Petterssen, S., 1936: Contribution to the theory of frontogenesis. *Geophys. Publ.*, **11** (6), 1–27.
- Reed, R. J., and F. Sanders, 1953: An investigation of the development of a mid-tropospheric frontal zone and its associated vorticity field. *J. Meteor.*, **10**, 338–349.
- Reeder, M. J., and D. Keyser, 1988: Balanced and unbalanced upper-level frontogenesis. *J. Atmos. Sci.*, **45**, 3366–3386.
- Rotunno, R., W. C. Skamarock, and C. Snyder, 1994: An analysis of frontogenesis in numerical simulations of baroclinic waves. *J. Atmos. Sci.*, **51**, 3373–3398.
- Sanders, F., 1988: Life history of mobile troughs in the upper west-lies. *Mon. Wea. Rev.*, **116**, 2629–2648.
- , 1993: Upper-level geostrophic diffluence and deepening of surface lows. *Wea. Forecasting*, **8**, 339–344.
- , L. F. Bosart, and C.-C. Lai, 1991: Initiation and evolution of an intense upper-level front. *Mon. Wea. Rev.*, **119**, 1337–1367.
- Schultz, D. M., and C. A. Doswell III, 1999: Conceptual models of upper-level frontogenesis in south-westerly and north-westerly flow. *Quart. J. Roy. Meteor. Soc.*, **125**, 2535–2562.
- Shapiro, M. A., 1981: Frontogenesis and geostrophically forced secondary circulations in the vicinity of jet stream-frontal zone systems. *J. Atmos. Sci.*, **38**, 954–973.
- , 1982: Mesoscale weather systems of the central United States. NOAA-CIRES Tech. Rep., University of Colorado, 78 pp. [Available from Cooperative Institute for Research in Environmental Sciences, University of Colorado-NOAA, Boulder, CO 80309.]
- Wandishin, M. S., J. W. Nielsen-Gammon, and D. Keyser, 2000: A potential vorticity diagnostic approach to upper-level frontogenesis within a developing baroclinic wave. *J. Atmos. Sci.*, **57**, 3918–3938.